Hindawi Publishing Corporation
International Journal of Spectroscopy
Volume 2012, Article ID 501706, 7 pages
doi:10.1155/2012/501706

Research Article

Application of Raman Spectroscopy to the Biooxidation Analysis of Sulfide Minerals

J. V. García-Meza,[1] R. H. Lara,[1,2] and H. R. Navarro-Contreras[3]

[1] *Geomicrobiology, Institute of Metallurgy, UASLP, Sierra Leona 550, Lomas 2°, 78210 San Luis Potosí, SLP, Mexico*
[2] *Electrochemical Area, Department of Chemistry, UAM-I, A.P. 55-534, 09340 Mexico, DF, Mexico*
[3] *Coordination for the Innovation and the Application of Science and Technology, UASLP, Sierra Leona 550, Lomas 2°, 78210 San Luis Potosí, SLP, Mexico*

Correspondence should be addressed to J. V. García-Meza, jvgm@uaslp.mx

Received 16 July 2011; Accepted 17 November 2011

Academic Editor: Rolf W. Berg

We report the application of confocal laser scanning microscopy CLSM and Raman spectroscopy on the (bio)chemical oxidation of pyrite and chalcopyrite, in order to understand how surface sulfur species (S_n^{2-}/S^0) affects biofilm evolution during mineral colonization by *Acidithiobacillus thiooxidans*. We found that cells attachment occurs as cells clusters and monolayered biofilms within the first 12 h. Longer times resulted in the formation of micro- and macrocolonies with variable cell density and higher epifluorescence signal of the extracellular polymeric substances (EPS), indicating double dynamic activity of *A. thiooxidans*: sulfur biooxidation and biofilm formation. Raman spectra indicated S_n^{2-}/S^0 consumption modification during biofilm evolution. Hence, cell density increase was primarily associated with the presence of S^0; the presence of refractory sulfur species on the mineral surfaces does not to affect biofilm evolution. The EPS of the biofilms was mainly composed of extracellular hydrophobic compounds (*vr. gr.* lipids) and a minor content of hydrophilic exopolysaccharides, suggesting a hydrophobic interaction between attached cells and the altered pyrite and chalcopyrite.

1. Introduction

Sulfide minerals (SMs) are the main source of base metals (e.g., Fe, Ni, Cu, Zn, and Pb) in the world. Most of SMs are semiconductors, and, in their crystalline phase, the orbitals of the atoms (sulfur and metal) form electronic bands with different energy levels; the highest fully occupied electron energy levels form the valence band. For SM as pyrite (FeS_2), the valence bands are orbitals from the metal atoms, while the valence bands of other SMs as chalcopyrite ($CuFeS_2$) are derived from both metal and sulfur orbitals [1]. In chalcopyrite, the Fe^{3+} ion and the protons (H^+) can remove electrons from the valence band; thus, chalcopyrite is soluble in acid. In contrast, pyrite is acid insoluble, as Fe^{3+} is its main oxidizing agent at high and low pH, as it has been described by Sand et al. [1] and Schippers and Sand [2]. These authors concluded in these reports that the mechanism and chemistry of SM oxidation are determined by such electronic structure as well as the acid solubility. In both reports, the same authors also proposed the corresponding dissolution mechanisms for acid soluble and acid insoluble SMs, defined as polysulfide and thiosulfate (bio)oxidative pathways, respectively. Accordingly, the oxidation of an acid insoluble SM proceeds via the thiosulfate mechanism by means of electron extraction, by the indirect attack of hydrated Fe(III) ions. The main reduced sulfur obtained is the thiosulfate, which via a series of subsequent reactions yields sulfate and protons (via tetrathionate and other polythionates) or elemental sulfur (S^0). The S^0 is a by-product produced in significant amounts (10–20%) during the chemical or electrochemical oxidation of pyrite at pH < 2, moderate temperature and pressure, and in the absence of microorganisms [2–5].

Additionally, for acid soluble MS, the oxidation via the polysulfide mechanism occurs by means of the M–S bond cleaving due to the H^+ activity before the sulfidic sulfur

is oxidized. In the recent report of Rohwerder and Sand [5], the oxidation via the polysulfide mechanism yielded more than 90% of S^0, as the main intermediate compound. The complete oxidation of SM occurs chemically and biologically, by microorganisms such as the sulfur oxidizers (SOMs, e.g., *Acidithiobacillus thiooxidans* and *A. caldus*), the iron oxidizers (IOMs, e.g., *Leptospirillum ferrooxidans*), or by *Acidithiobacillus ferrooxidans* which has both metabolic capacities (SOM and IOM). Consequently, the SMs are chemically oxidized by the oxidant Fe^{3+} (1), ion which is regenerated from the Fe^{2+} by IOMs (2)

$$FeS_2 + 8H_2O + 14Fe^{3+} = 15Fe^{2+} + 2SO_4{}^{2-} + 16H^+ \quad (1)$$

$$14Fe^{2+} + 3.5O_2 + 14H^+ = 14Fe^{3+} + 7H_2O \quad (2)$$

$$2S + 2O_2 = 2SO_4{}^{2-} \quad (3)$$

SOMs oxidize the intermediary $S_n{}^{2-}/S^0$ species released after the iron has been oxidized by IOMs (3). Thus, SOMs like *A. thiooxidans* play an important role in electron cycles of near-surface environments when IOMs are also present [6]. The most critical sulfur species is the S^0 since it may accumulate in the course of SM dissolution due to its stability under acidic conditions [7]. Actually, Crundwell [8] suggests that the action of the SOMs is to remove the sulfur formed on the surface of SM, which may form a barrier to subsequent diffusion of ferrous ions. Another central fact is that S^0 is exclusively oxidized by SOMs because this sulfur species is inert to abiotic oxidation in acidic environments [7]. Finally, SOMs also provide protons (bioacidification) to maintain Fe^{3+} in its oxidized state and to regenerate the protons consumed at the beginning of the (bio)oxidation of acid soluble SM, via the polysulfide mechanism [2]. The former explained why S^0 was generally added to promote the growth of SOMs like *A. thiooxidans* in some bioleaching process, where mixed strains of leaching microorganism are added [9]. Thus, the SOMs are of industrial interest because these species enhance the rate of dissolution of the SM as pyrite and chalcopyrite.

It is well known that "given their druthers, microorganisms prefer a community-based, surface-bound, sedentary lifestyle (as biofilm) to a nomadic existence" [10]. The bioleachers also spend most of their life cycle attached to the solid SM; thus, a chief discussed matter in bioleaching is related with the colonization of the SM surfaces by biofilms-forming microorganism. Biofilms are highly organized systems of microorganisms, embedded in a self-produced, gelatinous, and hydrated matrix, composed of extracellular polymeric substances (EPS), ions, gases, colloidal and particulate compounds, and open water channels. The EPS matrix represents 50–90% of the biofilm, and its secretion is an essential characteristic of the biofilm development, first and foremost for the initial attachment of the cells to the surface [11], for example, mineral particles.

Previous results obtained by our group clearly indicate that the SOM *A. thiooxidans* forms biofilms strongly attached to the surface of pyrite during the dynamic interfacial mechanisms of S^0 biooxidation [12], suggesting that the cell attachment is primarily controlled by the availability and nature of electroactive S^0 species formed in the surface of the acid-insoluble SM. We applied laser-induced Raman spectroscopy to analyze the major surface products of massive electrodes of pyrite previously electrooxidized (eMPE), during the colonization of SOM *A. thiooxidans*. Raman spectroscopy is a scattering technique that provides information on energy vibrational levels in molecules and lattice modes of crystals. Raman spectroscopy is a nondestructive and highly sensitive technique that allows spatial analysis of surfaces to determine many of their physical properties [13]. Raman spectroscopy has been applied to identify the surface oxidation products of SM, during abiotic [4, 14, 15] and biotic oxidation [5, 16, 17]. On the other hand, the combined use of Raman spectroscopy and electrochemical techniques has resulted in a powerful tool to investigate the macrooxidation products of refractory SM, such as chalcopyrite [15]. The advantage of this kind of analysis is to monitor the *in situ* stages of (bio)chemical changes, for instance, on $S_n{}^{2-}/S^0$ [14].

On the same line of work, in a series of previous papers [12, 17], we reported on the effect of electrooxidation of MS previous to the subsequent sulfur biooxidation by *A. thiooxidans* that forms biofilms on MS electrodes. This procedure was followed because (1) *A. thiooxidans* is not able to oxidize directly the SM, (2) a thicker biofilm was established on massive pyrite and chalcopyrite electrodes previously electrooxidized (MPE and MCE, resp.) after biotic assays rather than in the chemically altered MPE, and (3) this procedure allows a better formation of the $S_n{}^{2-}/S^0$ species on the electrode surface. These results were suggested by atomic force microscopy (AFM) analysis and corroborated by Raman spectroscopy [12, 17]. Bioleaching kinetics depends mainly on factors associated with the SM bacteria interfacial system [10, 18]; the attachment of bacteria (biofilms) onto SM surface is supported via extracellular polymeric substances (EPSs), and their chemical composition is an important factor in bioleaching systems [19, 20].

Considering the relevance of the interfacial stages of SM electrodes during the bacterial activity in the biofilm formation and bioleaching process, in this work, we compared the biofilm evolution process (cell density and EPS characteristics) as well as the $S_n{}^{2-}/S^0$ species development during pyrite and chalcopyrite biooxidation by *A. thiooxidans*. MPE and MCE electrodes were chosen because they exhibit contrasting acid soluble and acid insoluble properties, with the subsequent formation of a wide range and ratio of $S_n{}^{2-}/S^0$ species during their biooxidation. The expected results may allow the manipulation of SM dissolution rates in bioleaching processes, as a function of $S_n{}^{2-}/S^0$ species composition. Our results provide a new approach for the evaluation of leaching bacteria-sulfide systems.

2. Materials and Methods

Pyrite and chalcopyrite samples were, respectively, obtained from Zacatecas, Zac., and Charcas, San Luis Potosí, México.

The sampled pyrite purity is of ~99.2% wt, with minor amounts of chalcopyrite ($CuFeS_2$, 0.3% wt) and sphalerite (ZnS, 0.5% wt), whereas the chalcopyrite purity is of ~99.5% wt, with major impurity of SiO_2 (~0.5% wt). The reported compositions were established on the basis of mineralogical characterization performed after chemical analysis of total acid-digested SM samples, X-ray diffraction patterns (XRD), and scanning electron microscopy coupled to energy dispersive X-ray spectroscopy (SEM-EDS) analyses. Crystals of pyrite and chalcopyrite were selected for the construction of massive pyrite (MPE) and massive chalcopyrite electrodes (MCEs) of about 1.2–1.5 cm^2. The MPE and MCE pristine surfaces were then polished until mirror-like surfaces were reached. Afterwards, electrooxidation of each electrode was done by turn to obtain S^0/S_n^{2-} species directly from the mineral surfaces, under acidic conditions (pH 2). The MPE and MCE surfaces were electrochemically oxidized in acidified ATCC-125 (American Type Culture Collection) growing medium, using an autolab PGSTAT 30 coupled to a PC with a classic Pyrex glass three electrode cell, as described by Lara et al. [17]. Hence, the working electrode was the MPE or MCE, the counterelectrode is a graphite rod, and a saturated sulfate electrode is used as a reference (SSE, 0.615 V *versus* SHE, the Standard Hydrogen Electrode). The selected potentials for electrooxidation were 1.115 V and 0.865 V *versus* SHE (during 3600 s) for the MPE and MCE, respectively, in agreement with previous electrochemical analysis (data not shown). The formation of S_n^{2-}/S^0 species was then confirmed on the eMPE and eMCE surfaces (Figure 2).

Acidithiobacillus thiooxidans (strain ATCC-8085) was cultivated aerobically at 28–30°C and 150 rpm in an Erlenmeyer flask with 50 mL of a specific media (ATCC-125); the pH was adjusted at 2 with concentrated H_2SO_4. For the bioassay, inoculums of *ca*. 10^8 cells/mL were transferred to flasks with 100 mL of culture media, pH 2 without a source of S^0; an electrooxidized electrode (eMPE or eMCE) was added to the system. The systems were incubated as previously described, during 1, 12, 24, and 120 h. These biotic assays were done in triplicate; an "abiotic" (uninoculated) control was also carried out in triplicate to compare between chemical and biological oxidation of S^0/S_n^{2-}. After each time, the obtained eMPEs and eMCEs were collected, dried with a direct current of nitrogen, and preserved in a desiccator under inert conditions until their analysis.

Raman and confocal laser scanning microscopy (CLSM) analyses were carried out for pristine MPE and MCE, electrooxidized surfaces (eMPE and eMCE without leaching), and after 1, 12, 24, and 120 h of assays in the biotic and the abiotic systems, to evaluate the evolution of interfacial processes associated with five stages of mineral colonization by *A. thiooxidans* (see below). For CLSM observations, the biofilms were previously fixed with formaldehyde (3%), stained during 75 min of incubation (at 30°C under dark conditions) using 0.1 g/L of lectin *Canavalia ensiformis* (Con-A; tetramethylrhodamine conjugated; Molecular Probes, Eugene, OR, USA) to stain extracellular and hydrophilic polysaccharides (α-mannose and α-glucose). Afterwards, biofilms were rinsed with HEPES (N-2-hydroxyethylpiperazine-N9-2-ethanesulfonic acid, at) buffer and stained with the lipophilic fluorescent stain Nile Red (NR; Sigma Aldrich; 10 mM and pH 7.4) for hydrophobic domains (as lipids) composing EPS; after 10 min at 30°C in the dark, the surfaces were rinsed again with HEPES to remove the excess of staining reagents. After cells staining, the electrode surfaces were examined using a CLSM (Leica DMI4000Bt) with a 63x immersion objective. CLSM images were acquired in two dimensions (2d). Con-A was excited at 488 nm, and the emitted signal was detected using a band pass filter for emission at 575 nm; NR was excited 515–560 nm; emission, >590 nm. The relative signal intensity of three groups of in-depth measurements was resolved using the software program of the CLSM (Leica LAS AF). The data were corrected for background signal. The intensity of Con-A and NR fluorescence was used to estimate the relative contribution of extracellular and hydrophilic polysaccharides (stained with Con-A) and hydrophobic EPS (stained with NR) to biofilm; the data were expressed in arbitrary units (A.U.). It has been demonstrated that CLSM is useful to quantify EPS in biofilms [21] and that CLSM is more sensitive than the chemical extraction of EPS in young and less compact biofilms.

Raman analysis was carried out in pristine and electrooxidized MPE and MCE (before the assay) and in eMPE and eMCE after 1, 12, 24, and 120 h of assays in biotic and abiotic systems. These analyses were performed using a triple monochromator Jobin Yvon T64000 spectrometer equipped with an optical microscope (Olympus BH2-UMA). Mineral surfaces were excited by an Ar^+ laser beam at 514 nm (Stabilité 2017, Spectra Physics). Collection time was 60 s in each analysis. At least 10 Raman spectra were collected from each surface. Raman performance and calibration were validated using a Si wafer by observing the well-known Si-LO single sharp peak at 521 cm^{-1}. Raman backscattering showed a signal/noise ratio greater than 100 for Si analysis, ensuring a good Raman performance during mineral analysis [17]. The vibrational range analyzed was 100–750 cm^{-1}, as the S^0/S_n^{2-} species show their main active modes within this interval (e.g., [6, 21]).

3. Results and Discussion

CLSM study confirmed the presence of cell clusters since the first hour attached onto the eMPE and eMCE surfaces (Figure 1), and the later formation of monolayered biofilms after 24 h in the eMPE (Figure 1(e)) and at 12 h in the eMCE (Figure 1(f)). However, higher cell densities were always observed in the eMCE than in the eMPE. In particular, at 120 h, in the eMPE, CLSM analysis confirmed the progressive senescence of biofilms on the surface, and only dispersed attached cells were observed (Figure 1(d)); meanwhile a multilayered biofilm was observed in the eMCE, which was mainly composed by extracellular hydrophobic compounds *vr*. *gr*. lipids (Figure 1(h), Table 1).

All former results are in agreement with those obtained by Raman spectroscopy (Figure 2). A summary of Raman transitions for identification of the corresponding S_n^{2-}/S^0 species is listed in Table 2. In all cases, Raman peaks at 343 and 381 cm^{-1}, and 289 cm^{-1} typically indicated pristine pyrite and chalcopyrite, respectively (Figure 2). The eMPE

Table 1: Epifluorescence of EPS of cells composing biofilms for the stages found in mineral colonization. Data: $n = 28$.

	Polysaccharides A.U.		Lipids A.U.	
Time	eMPE	eMPC	eMPE	eMPC
1 h	12.48	87.61	41.07	88.11
12 h	28.52	21.96	107.69	31.93
24 h	72.19	35.47	102.24	39.07
120 h	32.89	12.77	32.45	160.65

and eMCE surfaces before the assay (without leaching) showed additional Raman peaks at 155, 222, and 470 cm^{-1} and 150, 217, and 471 cm^{-1}, respectively, which indicated the formation of S^0-like species on both minerals (Figure 2, Table 2). The presence of such S^0-like species during the chalcopyrite oxidation has been demonstrated by Nava et al. [22]. A broad Raman peak asymmetry around 470-471 cm^{-1} (Figure 2) strongly suggested the formation of minor amounts of S_n^{2-} species (Table 2), together with S^0-like species in the eMPE. Former results indicated that eMPE and eMCE surfaces initially contained S_n^{2-}/S^0 species.

Raman spectra for the eMPE of the abiotic control after 1 h showed the presence of S^0/S_n^{2-} because the associated Raman peaks at 155, 222, and 455–475 are a clear signature of these species (Figure 2, Table 2) as mentioned above. Additionally, the Raman spectra for the eMPE after 1 h in the biotic trial clearly indicate the formation of very well crystallized S^0 (sharp peaks at 155, 222, and 470 cm^{-1} and minor peaks at 245 and 437 cm^{-1}). These results could be indicative of initial stages of S^0/S_n^{2-} biooxidation followed by the modification of these crystalline structures. In comparison, Raman spectra for the eMCE of the abiotic control after 1 h showed the presence of S_n^{2-} and covellite (CuS), according with the Raman peak position and its broadened asymmetric shape around 470 cm^{-1} (Figure 2, Table 2). Meanwhile, the Raman spectra for the eMCE surface after 1 h in biotic trial showed an increasing amount of S_n^{2-} as indicated by the coarse Raman peaks around 447–468 cm^{-1} (Figure 2, Table 2). Summarizing, at 1 h onto the eMPC surface, limited S^0/S_n^{2-} consumption was associated with scant bacterial mineral colonization (Figure 1(a)); nevertheless, a better crystallization of S^0 species was found in the biotic surfaces (Figure 2). These results suggest that initial cells clustering occur via (bio)chemical modification of sulfur crystal lattices, as indicated by Rohwerder and sand [5]. In contrast, higher cell density was observed on eMCE surface after 1 h of biotic assay (Figure 1(e)) as well as a total depletion of S^0, resulting in a wide range of S_n^{2-} species on biooxidized surfaces (Figure 2).

After 12 h of biooxidation, it was observed clusters of attached cells forming monolayered biofilms on eMPE (Figure 1(b)); the results of Raman analysis suggested that the bacteria were performing a dynamic sulfur oxidize activity, since it was recorded a partial depletion of S_n^{2-} (coarse peaks at 456–471 cm^{-1}) and a total depletion of S^0 (Figure 2). Meanwhile, Raman spectra collected from the abiotic control indicated a better crystallization of S^0 and

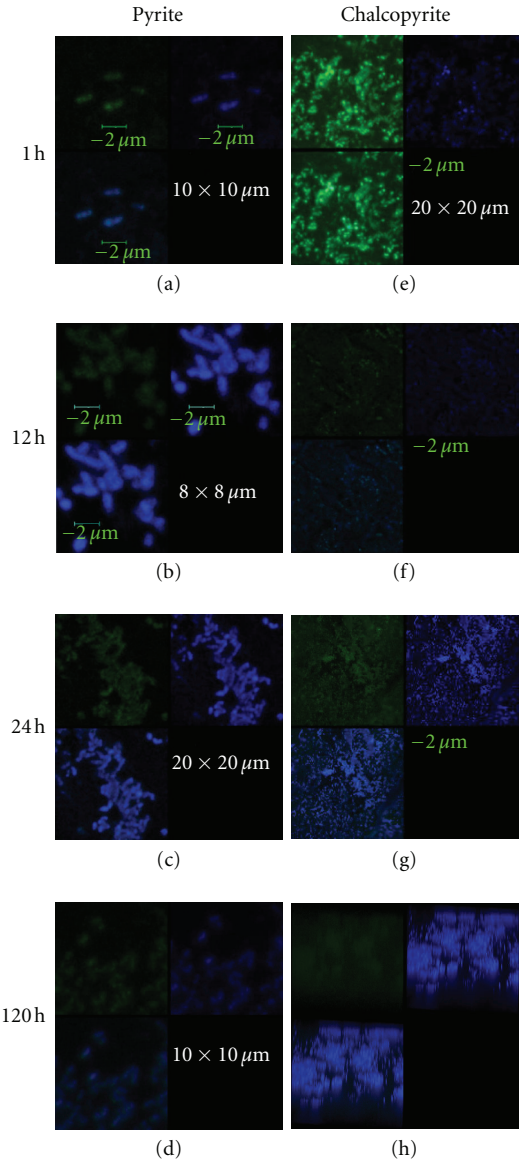

Figure 1: CLSM images of *A. thiooxidans* cells (2D) after biooxidation of eMPEs (first column) and eMCEs (second column) surfaces after 1 h (first line), 12 h (second), 24 h (third), and 120 h (fourth). Epifluorescence of exopolysaccharides (in green colour) and of lipids (in blue). An overlap of both epifluorescence images is presented in the low left side of each set of images.

minor amounts of S_n^{2-}, since Raman peaks at 155, 222, and 455–473 cm^{-1} are sharp and well defined (Figure 2; Table 2). For the eMCE, the epifluorescence of EPS decreased (Table 1) but not the cell density (Figure 2(f)); the former maybe because the remaining presence of S_n^{2-} species could be less available for biooxidation, as the coarse peak around 468 cm^{-1} on the eMCE suggested (Figure 2, Table 2). In contrast, Raman spectra collected from the abiotic control after 12 h of assay indicated the formation of very well crystallized S^0-like species, since Raman peaks at 150, 216, and 470 cm^{-1} are well defined (Figure 2; Table 2). In general overview, Raman results confirmed the occurrence of

Table 2: Summary of Raman transitions identification in terms of main sulfur species on MPE, eMPE, MCE, and eMCE surfaces. (Vn): order of importance in Raman transitions.

Species	Raman peak position (cm^{-1})	Reference
Pyrite (monosulfide, S^-)	344 (v2), 380 (v1), 433 (v3)	[4, 21]
	353, 387	[6]
Chalcopyrite (monosulfide, S^-)	289 (v1), 320 (v3), 471 (v2)	[15, 16]
Polysulfides (S_n^{2-})	from 443 to 480, main at 470 (v1)	[4, 15, 21]
Elemental sulfur (S^0)	150 (v3), 222 (v2), 470 (v1)	[4, 21]
Covellite (CuS, S^-)	267 (v2), 474 (v1)	[14–16]

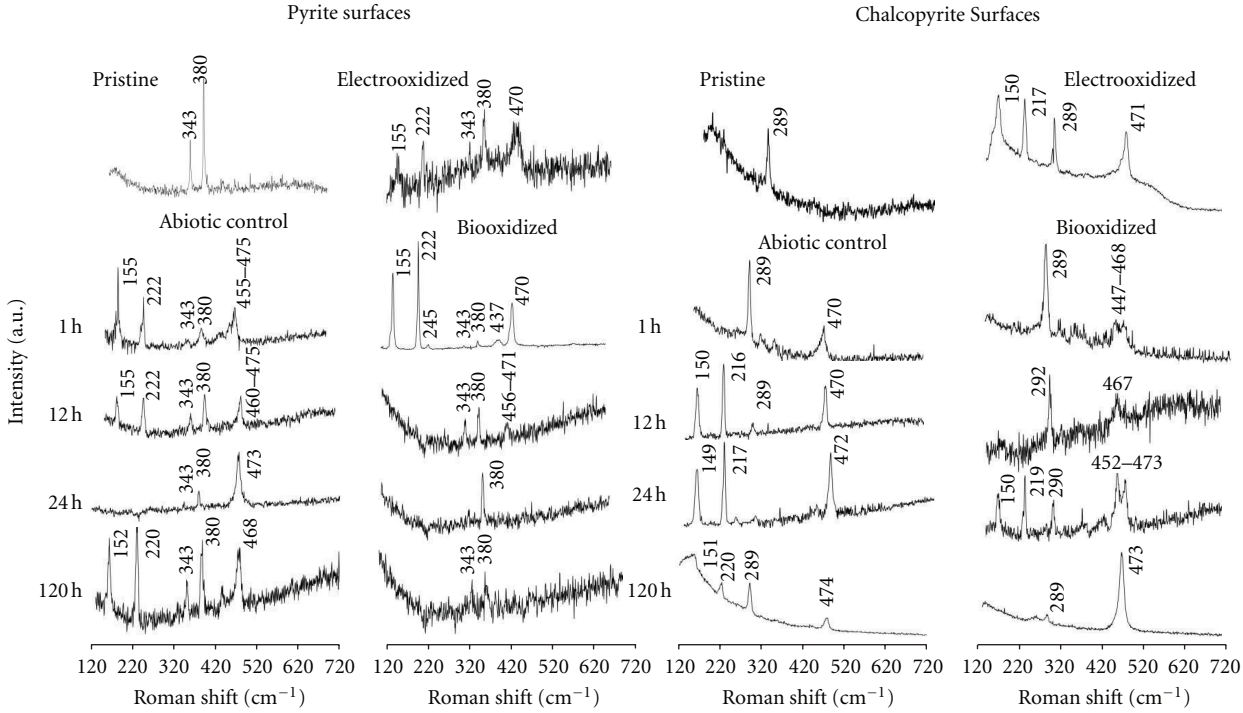

Figure 2: Raman spectra collected on abiotic control and biooxidized of eMPE surfaces (first and 2nd columns) and on abiotic control and biooxidized eMCE surfaces (3rd and 4th columns), after 1, 12, 24, and 120 h of immersion. 60 s of collection time. $\lambda = 514$ nm.

S^0/S_n^{2-} biooxidation on studied minerals due to biological activity of *A. thiooxidans* after 12 h, and they are clear evidence that illustrates the progressive depletion of S^0/S_n^{2-} on altered surfaces, even when some surface species are refractory.

After 24 h of biotic assay, it was observed biofilms of *A. thiooxidans* with two layers of cells onto the eMPE surface (Figure 1(c)), but also a total depletion or consumption of S_n^{2-}/S^0 (Figure 2); this apparent conditions of starvation and a high cell density may promote the transition from surface-attached cells into a mature biofilm. In contrast, Raman spectra collected in the abiotic controls after 24 h showed an intense sharp peak at 455–475 cm^{-1}, indicating the main formation of S_n^{2-} species in most of oxidized mineral areas (Figure 2; Table 2). Sasaki et al. [6] also found the total disappearance of the peaks associated with the S–S of S^0 (150, 220, and 470 cm^{-1}) when *A. thiooxidans* was grown on pretreated pyrite with Fe^{3+} ions, and the presence of such peaks in the abiotic control or in biotic assay but with *A. ferrooxidans*; their results were obtained after 72 h. We decided to compare such results performing the assays at 72 h, and we obtained similar Raman spectra to that at 24 h for the eMPE (data not shown). In contrast, Raman spectra obtained on the eMCE surface after 24 h of biotic assay showed intense and sharp peaks at 150, 219, and 452–473 cm^{-1}, which evidenced the formation of a wide range of S_n^{2-} species and minor amounts of S^0 (Figure 2, Table 2). In addition, Raman spectra collected in the abiotic control after 24 h showed intense sharp peaks at 149, 217, and 472 cm^{-1}, indicating the formation of S^0 species on oxidized chalcopyrite (Figure 2; Table 2). The remaining presence of S_n^{2-} species on eMCE within the first 24 h on biooxidized surface, and the total consumption of S_n^{2-}/S^0 species on eMPE at this same biooxidation time (Figure 2) suggest that some S_n^{2-} species are refractory, and its biooxidation occurs slowly on chalcopyrite system. In spite of this, biofilms organization results in the development of macrocolonies (Figure 1(g)).

Finally, the CLSM observation after 120 h of exposure of *A. thiooxidans* to the eMPE surface confirmed the progressive decrease of biofilms, and only dispersed attached cells were observed (Figure 1(d)). The senescence of such biofilm is explained with the Raman analysis, which showed low intensity and noisy peaks, similar to those obtained in the pristine MPE surfaces (Figure 2). Thus, the S^0 species were totally consumed by the microorganism after 120 h. Meanwhile in the abiotic control and after 120 h, continues the formation of S_n^{2-}/S^0 species (Figure 2). In contrast, the CLSM analysis after 120 h of exposure of *A. thiooxidans* to the eMCE surface still showed the presence of macrocolonies (Figure 1(h)), whereas Raman analysis indicated the formation of covellite species which do not significantly affected the biofilm evolution (Figure 2, Table 2). In the abiotic control, S_n^{2-}/S^0 species remain after 120 h (Figure 2, Table 2). Previous results suggested that the decrease of biofilms on chalcopyrite surface is a much slower process than on pyrite, probably associated with a more abundant formation of S_n^{2-}/S^0 species, some refractory, due to the soluble-acid characteristics of this SM.

The Raman results discussed above suggested a periodic formation of variable amounts of S^0/S_n^{2-} species on the altered pyrite (eMPE) and chalcopyrite (eMCE), only restricted by kinetic processes. Some S^0 species are progressively oxidized to sulfate ions, whereas S_n^{2-} produced S^0 (and covellite for chalcopyrite) due to oxidizing conditions in the surrounding acidic medium. The rate of synthesis/consumption strongly differs because of the specific acid solubility of each SM. Since, in our experiment, the initial Fe^{2-}/Fe^{3+} ratio was the same in all the biotic and abiotic trials (0.01 g of iron), the previous described results are mainly a consequence of the biooxidation of the S^0 generated on the eMPE and eMCE; but also because the acid solubility of the chalcopyrite in the biotic and abiotic trials, since the protons (H^+) remove electrons (oxidize) from the valence band of both cupper and sulfur orbitals [2], resulting in a higher amount of S_n^{2-}/S^0 species than in the acid-insoluble pyrite. The stability of low amounts of S^0/S_n^{2-} species (10–20%) on eMPE and of high amounts of S^0/S_n^{2-} species (*ca*. 90%) on eMCE during chemical or electrochemical oxidation, has been previously indicated under acidic conditions [2, 4, 6, 23]. Consequently, the eMPEs and eMCEs here prepared were adequate interfaces for inducing the mineral colonization by the sulfur-oxidizing *A. thiooxidans*.

Epifluorescence analysis indicated variable secretion of hydrophilic exopolysaccharides and hydrophobic EPS (as lipids) for the four stages traversed during the biofilms evolution (Table 1). After 1 h of biooxidation, it was found a significant EPS production, especially in the eMCE surfaces (Table 1), where in hydrophilic exopolysaccharides were almost 8 times and hydrophobic EPS were 2 times more than in eMPE. Longer times of biooxidation implied changes in the epifluorescence of these EPS; the maximum secretion of EPS in the colonized eMPE was achieved at 12 h (hydrophobic EPS) and 24 h (hydrophilic exopolysaccharides); whereas in the biofilm developed on the eMCE surfaces, the maximum secretion was obtained at 24 (hydrophilic exopolysaccharides) and 120 h (hydrophobic EPS). This higher content of EPS is related with the increase of the cell density but also with the establishment of a self-covered matrix of EPS in biofilms (Figure 1). The data of epifluorescence also indicated that EPS mainly comprises hydrophobic domains as lipids (Table 1), in both colonized eMPE and eMCE surfaces.

4. Conclusions

We found that *A. thiooxidans* colonizes and forms biofilms on the surface of the MPE and MCE previously electrooxidized (eMPE and eMCE, resp.), since the first hour of contact. At this stage, eMPE was scantly colonized, whereas eMCE comprises a higher cell density within biofilms. The cell colonization and consequently the biooxidation of eMCE were more favored processes, despite the formation of refractory sulfur species such as S_n^{2-} and some of covellite. Indeed, the number of attached cells was always higher on eMCE than on the eMPE surfaces, due to a more significant formation and availability of S_n^{2-}/S^0 species. Longer biooxidation time resulted in the formation of macrocolonies, process widely favored on eMCE surfaces. Epifluorescence analysis of attached cells indicated progressive secretion of hydrophilic exopolysaccharides and hydrophobic domains as lipids in EPS for all the stages of biofilms evolution. The highest secretion of these substances was observed during chalcopyrite colonization (around 24 h). The presence of hydrophobic sulfur substances (S_n^{2-}/S^0) as well as the major contribution of hydrophobic domains (as lipids) in EPS suggested that bacterial attachment to oxidized minerals was a hydrophobic interaction.

Acknowledgments

Financial support for this work comes from the Mexican Council of Science and Technology (CONACyT, Project no. 05-49321). The authors thank MS Keila N. Alvarado and Dr. Amauri Pozos (Basics Sciences Laboratory, UASLP) for access of the CLSM equipment. The authors also thank Erasmo Mata-Martinez for mineral section preparation and Francisco Galindo-Murillo for MPE preparation. R. H. Lara also thanks CONACyT for his postdoctoral fellowship.

References

[1] W. Sand, T. Gehrke, P.-G. Jozsa, and A. Schippers, "(Bio)chemistry of bacterial leaching-direct vs. indirect bioleaching," *Hydrometallurgy*, vol. 59, no. 2-3, pp. 159–175, 2001.

[2] A. Schippers and W. Sand, "Bacterial leaching of metal sulfides proceeds by two indirect mechanisms via thiosulfate or via polysulfides and sulfur," *Applied and Environmental Microbiology*, vol. 65, no. 1, pp. 319–321, 1999.

[3] I. C. Hamilton and R. Woods, "An investigation of surface oxidation of pyrite and pyrrhotite by linear potential sweep voltammetry," *Journal of Electroanalytical Chemistry*, vol. 118, pp. 327–343, 1981.

[4] J. R. Mycroft, G. M. Bancroft, N. S. McIntyre, J. W. Lorimer, and I. R. Hill, "Detection of sulphur and polysulphides on

electrochemically oxidized pyrite surfaces by X-ray photoelectron spectroscopy and Raman spectroscopy," *Journal of Electroanalytical Chemistry*, vol. 292, no. 1-2, pp. 139–152, 1990.

[5] T. Rohwerder and W. Sand, "The sulfane sulfur of persulfides is the actual substrate of the sulfur-oxidizing enzymes from *Acidithiobacillus* and *Acidiphilium* spp," *Microbiology*, vol. 149, no. 7, pp. 1699–1710, 2003.

[6] K. Sasaki, M. Tsunekawa, T. Ohtsuka, and H. Konno, "The role of sulfur-oxidizing bacteria Thiobacillus thiooxidans in pyrite weathering," *Colloids and Surfaces A*, vol. 133, no. 3, pp. 269–278, 1998.

[7] T. Rohwerder and W. Sand, "Mechanisms and biochemical fundamentals of bacterial metal sulfide oxidation," in *Microbial Processing of Metal Sulfides*, E. R. Donati and W. Sand, Eds., pp. 35–58, Springer, New York, NY, USA, 2007.

[8] F. K. Crundwell, "How do bacteria interact with minerals?" *Hydrometallurgy*, vol. 71, no. 1-2, pp. 75–81, 2003.

[9] Y.-G. Liu, M. Zhou, G.-M. Zeng et al., "Bioleaching of heavy metals from mine tailings by indigenous sulfur-oxidizing bacteria: effects of substrate concentration," *Bioresource Technology*, vol. 99, no. 10, pp. 4124–4129, 2008.

[10] W. M. Dunne Jr., "Bacterial adhesion: seen any good biofilms lately?" *Clinical Microbiology Reviews*, vol. 15, no. 2, pp. 155–166, 2002.

[11] T. R. Neu, A. Eitner, and M. L. Paje, "Development and architecture of complex environmental biofilm- Lotic Biofilm Systems," in *Fossil and recent Biofilms: A natural History of Life on Earth*, D. M. Paterson and G. A. Zavarzin, Eds., pp. 29–45, Kluwer Academic, Amsterdam, The Netherlands, 2003.

[12] D. M. González, R. H. Lara, D. Valdez-Pérez et al., "Evolution of biofilms during the colonization process of pyrite by *Acidithiobacillus thiooxidans*," *Applied Microbiology and Biotechnology*, vol. 93, no. 2, pp. 763–775, 2012.

[13] H. Navarro-Contreras, A. G. Rodríguez, M. A. Vidal, M. Rojas-López, and H. Pérez Ladrón de Guevara, "Application of Raman spectroscopy to the determination of physical properties of semiconductor films," Submitted.

[14] S. B. Turcotte, R. E. Benner, A. M. Riley, J. Li, M. E. Wadsworth, and D. M. Bodily, "Surface analysis of electrochemically oxidized metal sulfides using Raman spectroscopy," *Journal of Electroanalytical Chemistry*, vol. 347, no. 1-2, pp. 195–205, 1993.

[15] G. K. Parker, R. Woods, and G. A. Hope, "Raman investigation of chalcopyrite oxidation," *Colloids and Surfaces A*, vol. 318, no. 1–3, pp. 160–168, 2008.

[16] K. Sasaki, Y. Nakamuta, T. Hirajima, and O. H. Tuovinen, "Raman characterization of secondary minerals formed during chalcopyrite leaching with *Acidithiobacillus ferrooxidans*," *Hydrometallurgy*, vol. 95, no. 1-2, pp. 153–158, 2009.

[17] R. H. Lara, D. Valdez-Pérez, A. G. Rodríguez, H. R. Navarro-Contreras, R. Cruz, and J. V. García-Meza, "Interfacial insights of pyrite colonized by *Acidithiobacillus thiooxidans* cells under acidic conditions," *Hydrometallurgy*, vol. 103, no. 1–4, pp. 35–44, 2010.

[18] K. Harneit, A. Göksel, D. Kock, J. H. Klock, T. Gehrke, and W. Sand, "Adhesion to metal sulfide surfaces by cells of *Acidithiobacillus ferrooxidans*, *Acidithiobacillus thiooxidans* and *Leptospirillum ferrooxidans*," *Hydrometallurgy*, vol. 83, no. 1–4, pp. 245–254, 2006.

[19] K. Kinzler, T. Gehrke, J. Telegdi, and W. Sand, "Bioleaching: a result of interfacial processes caused by extracellular polymeric substances (EPS)," *Hydrometallurgy*, vol. 71, no. 1-2, pp. 83–88, 2003.

[20] W. Zeng, G. Qiu, H. Zhou et al., "Characterization of extracellular polymeric substances extracted during the bioleaching of chalcopyrite concentrate," *Hydrometallurgy*, vol. 100, no. 3-4, pp. 177–180, 2010.

[21] V. Toniazzo, C. Mustin, J. M. Portal, B. Humbert, R. Benoit, and R. Erre, "Elemental sulfur at the pyrite surfaces: speciation and quantification," *Applied Surface Science*, vol. 143, no. 1, pp. 229–237, 1999.

[22] D. Nava, I. González, D. Leinen, and J. R. Ramos-Barrado, "Surface characterization by X-ray photoelectron spectroscopy and cyclic voltammetry of products formed during the potentiostatic reduction of chalcopyrite," *Electrochimica Acta*, vol. 53, no. 14, pp. 4889–4899, 2008.

[23] T. Biegler and D. A. Swift, "Anodic electrochemistry of chalcopyrite," *Journal of Applied Electrochemistry*, vol. 9, no. 5, pp. 545–554, 1979.